JOURNAL OF AIRCRAFT
Vol. 43, No. 1, January–February 2006

Integrated Multidisciplinary Topology Optimization Approach to Adaptive Wing Design

K. Maute*
University of Colorado at Boulder, Boulder, Colorado 80309-0429
and
G. W. Reich†
U.S. Air Force Research Laboratory, Dayton, Ohio 45433-7531

This paper presents a novel optimization approach to the design of mechanisms in morphing aircraft structures. The layout of the mechanism and the location and number of actuators and pivots are determined by an extended formulation of a material-based topology optimization. The design problem is modeled within a coupled fluid-structure analysis framework to directly assess aerodynamic performance criteria while optimizing the overall mechanized system. The proposed methodology is illustrated through the design optimization of a quasi-three-dimensional section of an adaptive wing, where the approach is compared to a conventional two-step approach of first optimizing the aerodynamic shape for one or multiple flight conditions, and then finding the mechanism that leads to this shape. The comparison shows that the interactions between flow, structural deformation, mechanism, and actuator must be considered to find the optimal solution. The optimization approach presented allows direct consideration of these interactions at the expense of an increased computational burden.

Nomenclature

$\mathcal{A}$	=	aeroelastic Jacobian
a	=	dimension of airfoil section
$\boldsymbol{a}$	=	vector of adjoint solution
$\boldsymbol{a}_u$	=	structural contribution to $\boldsymbol{a}$
$\boldsymbol{a}_v$	=	contribution of $\boldsymbol{v}$ to $\boldsymbol{a}$
$\boldsymbol{a}_w$	=	flow contribution to $\boldsymbol{a}$
b	=	dimension of airfoil section
c	=	dimension of airfoil section
c_j	=	generic optimization criterion
$\mathcal{D}$	=	fluid mesh motion equations
D	=	aerodynamic drag
E	=	Young's modulus
$\mathcal{F}$	=	flow equations
$F_i^{\max}$	=	maximum actuator force
$\boldsymbol{F}_i^{\text{act}}$	=	force generated by ith actuator
k	=	spring stiffness
L	=	aerodynamic lift
$M_{\max}$	=	maximum pitching moment
M_{pitch}	=	aerodynamic pitching moment
Ma	=	free-stream Mach number
$m_{\max}$	=	maximum mass
N^{act}	=	number of actuators
p_∞	=	free-stream pressure
q	=	aerodynamic pressure
r_i	=	resource parameter
$\mathcal{S}$	=	structural equilibrium equations
s_i	=	generic optimization variable
t_{skin}	=	skin thickness
t_{web}	=	web thickness
$\boldsymbol{u}$	=	structural displacements
$u_{\max}$	=	maximum stroke
$\boldsymbol{v}$	=	motion of fluid grid points
w	=	width of airfoil section
$\boldsymbol{w}$	=	fluid state variables
$\boldsymbol{x}$	=	vector of spatial coordinates
$\boldsymbol{x}_{\text{skin}}^a$	=	target position of skin nodes
$\boldsymbol{x}_{\text{skin}}^d$	=	position of skin nodes in deformed state
α	=	angle of attack (pitch)
β	=	exponent in SIMP formulation
ν	=	Poisson ratio
ρ	=	material density
ρ_∞	=	free-stream density
χ	=	indicator function
Ω	=	design domain
Ω_m	=	set of all material points

Presented as Paper 2004-1805 at the Adaptive Structures Conference, Palm Springs, CA, 19–22 April 2004; received 11 August 2004; revision received 2 January 2005; accepted for publication 22 January 2005.

*Assistant Professor, Department of Aerospace Engineering Sciences, Center for Aerospace Structures; maute@colorado.edu. Member AIAA.

†Research Aerospace Engineer, Air Vehicles Directorate; Gregory.Reich@wpafb.af.mil. Member AIAA.

I. Introduction

VEHICLE morphing has the potential to greatly increase the capability of aircraft systems. Adapting the wing shape in flight would enable an air vehicle to perform multiple tasks in a single mission, radically expanding its flight envelope. A vehicle's shape can be adapted, for example, by sweeping or twisting the wing or by changing its span and area. Other morphing concepts include changing the wing camber and the distribution of camber along the span. The significant advantages of the latter concept were demonstrated by the Mission Adaptive Wing Program[1] in the 1980s. Generally, however, the complexity of integrating actuators and mechanisms into the wing structure and a lack of energy- and weight-efficient actuation devices have prevented this concept from leaving the experimental state and becoming a practical technology.

Researchers are in the process of addressing these issues. In the past decade, significant improvements have been made in actuation technology, including the use of active materials directly or through integration into systems such as compact hybrid actuators.[2–4] High-energy-density actuation systems have been realized by coupling the strengths of active materials with the robustness of traditional hydraulic and pneumatic actuation systems. This combination has created a class of actuators capable of delivering the power and stroke required for aircraft-scaled actuation in a smaller-sized package.

As the actuator design itself has improved, researchers have continued to investigate the integration of actuators for changing the wing shape, and their work has resulted in two main concepts:

multiply-redundant control surfaces[5] and conformal shape changes.[6] The former employs multiple traditional control surfaces to change the aerodynamic shape, where the optimal number, location, and size of the surfaces are unknowns. It uses mature technology to actuate the surfaces but may have significant drawbacks with respect to aerodynamic drag and radar signature. The latter method is to deform the airfoil section in a conformal, quasi-elastic fashion. Conformal shape changes can be obtained either by distributed actuation concepts, such as active materials, or by conventional designs based on discrete actuators combined with mechanisms.[7–9] The energy density and the limited force and/or stroke generation capabilities of today's active materials are insufficient when significant global shape changes are required.[5] Therefore, discrete actuators are still the favorable option for generating large shape changes in which the actuation stroke and force are transferred to the skin of the wing by mechanisms. A combination of multiply-redundant, conformal control surfaces has also been demonstrated.[10]

Despite these advances, a sufficient understanding of the *design* of shape-adaptive wings, including the definition of appropriate performance measures that assess different designs, is still lacking. The performance measures need to capture the tradeoff between resources spent to adapt the wing and aerodynamic payoffs over the desired flight envelope.[11]

A. Adaptive Wing Design

At its most fundamental level, an adaptive airfoil section includes a skin, a support structure, and a mechanism. Any process to create an adaptive airfoil design must include these elements, and all of the components need to be designed in concert with each other. Additionally, the number, type, and location of actuators need to be determined. Nonlinear fluid–structure interactions need to be included, because aerodynamic loads are strongly dependent on structural displacements, which include actuation modes and elastic deformation. In addition, aerodynamic and structural design criteria must be considered simultaneously to obtain a good solution.

It is easy to see that the design of adaptive wings is a truly multidisciplinary problem. It calls for the merger of aerodynamic shape optimization, structural and mechanism design, and the optimal placement of actuators, all in a design environment that accounts for fluid–structure interaction. Aerodynamic shape optimization[12,13] and high-fidelity aeroelastic analysis and design[14–16] have been extensively studied in the aeronautical community. Topology optimization has been applied to a broad range of structural optimization and multiphysics problems,[17–19] including the design of aeroelastic wing structures.[20,21] The design of mechanisms by topology optimization has also attracted substantial attention in the microelectromechanical systems community,[22–26] and the optimal placement of actuators has been studied in the context of smart structures and materials.[27,28]

The present study investigates the fusion of the above disciplines. This fusion can happen sequentially, or in a simultaneous process that determines external airfoil shape, internal mechanism layout, and actuator position, direction, and magnitude in one step.

B. Two-Step Approach

A simple approach to adaptive wing design consists of two sequential design and optimization steps. The first step is a purely aerodynamic analysis in which a set of optimum shapes is determined for a given set of flight conditions. The optimization process includes no information about the internal structure of the vehicle and is solely interested in the outer mold line (OML). The second step is to design a mechanism based on some internal structural layout that recreates those target shapes as accurately as possible.[9,29–33] Here the aerodynamic loads are considered as external boundary conditions, but typically the variation of those loads as the OML changes are ignored.

The main advantages of this approach are that design tools for the single disciplines already exist and the physics that governs each subproblem is well understood. However, there are a number of disadvantages to this approach. The second step requires the designer to match a target shape, which always results in a finite error, decreasing the realized performance of the system. Additionally, this approach does not account for actuator limitations, both in maximum force or stroke. It may be that the required shape is unrealizable due to these constraints. Most importantly, the interaction between fluid and mechanism affects both steps of the process.

C. Integrated Multidisciplinary Approach

The disadvantages of the two-step procedure can be overcome by embedding topology optimization for mechanism design into a fluid–structure analysis model. Instead of having two separate optimization procedures, a single optimization is done to find the design that meets the original performance requirements directly. This multidisciplinary optimization approach includes the physics of interaction between the mechanism/structure and the fluid. Additionally, it enables the simultaneous consideration of aerodynamic and structural design criteria as the objective and constraints. Aerodynamic criteria include lift, drag, and aerodynamic moments; structural criteria include the system mass and constraints on actuation energy, stroke, and maximum force.

To predict the aerodynamic and structural design criteria and to account for fluid–structure interaction, the coupled fluid–structure response is predicted by a high-fidelity numerical simulation method. The structure is modeled by a geometrically nonlinear finite element formulation to account for large displacements generated by the resultant mechanism. The aerodynamic loads are predicted by a three-dimensional finite volume method.

In this paper, the proposed integrated multidisciplinary topology optimization addresses the design of mechanisms and placement of actuators in the context of an adaptive wing section design. The paper is organized as follows: in Sec. II, the mechanism design problem is formulated as a topology optimization problem; in Sec. III, the coupled fluid–structure analysis and sensitivity analysis framework is outlined. The advantages of the proposed integrated approach versus a conventional two-step method are illustrated by a numerical example in Sec. four.

II. Problem Formulation

The essential components for camber variation of an adaptive wing section are illustrated by the model shown in Fig. 1. A kinematic mechanism transfers actuation forces to a deformable skin that carries aerodynamic pressure loads back to the internal structure. The mechanism consists of rigid or flexible members, hinges, and pivots at which the mechanism is attached to the support structure. The support structure plays the role of traditional ribs and spars, carrying primary loads back to the fuselage.

In the following, only the shape of the support structure is assumed to be known, as the design of this component is typically driven by the overall wing stiffness requirements. The proposed optimization methodology determines the layout of the mechanism structure, the pivot points, and the location and direction of actuator loads. The resulting design problem is cast as an extended material-based topology optimization problem.

A. Material-Based Topology Optimization

Topology optimization methods allow a designer to generate almost arbitrary geometries, specifying only the design domain, Ω; an

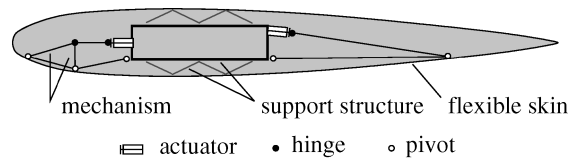

a) Initial configuration

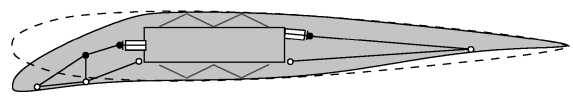

b) Actuated configuration

Fig. 1 Design of an adaptive airfoil—model problem.

initial design is not required. The most general approach for formulating the topology optimization problem relies on an on/off material distribution describing the geometry of the structure, as shown in Fig. 2. This distribution can be written as follows, with χ being a binary indicator function:

$$\chi(\boldsymbol{x}) = \begin{cases} 1 & \forall \boldsymbol{x} \in \Omega_m \\ 0 & \forall \boldsymbol{x} \in \Omega / \Omega_m \end{cases} \tag{1}$$

where $\boldsymbol{x}$ denotes a spatial coordinate and Ω_m is the set of all material points. Discretization of this formulation by finite elements leads to an ill-posed integer optimization problem. Regularization is done by introducing porous material models where the material's density serves as a design variable. Although porous material models with extreme properties are necessary to obtain a well-posed optimization problem, they lead to impractical optimization results with little physical significance.

For these reasons, the solid isotropic material with penalization (SIMP) approach has become popular in the engineering optimization community. The SIMP approach relates the Young's modulus E to the density ρ[34,35] as follows:

$$E(\rho) = (\rho/\rho_0)^{\beta} E_0, \qquad \beta \geq 3 \tag{2}$$

where the subscript "0" denotes the properties of the bulk material. When maximizing the structural stiffness while constraining the system mass, the nonlinearity of the SIMP model penalizes intermediate densities and leads to an approximate "0–1" material distribution in the design domain. These material distributions can then be transferred into a structural design, either manually or in an automated fashion. [36,37] However, because the results of the SIMP approach depend on the orientation and refinement of the mesh, the formulation of the optimization problem needs to be augmented by additional regularization methods. [38,39]

B. Design of Mechanisms by Topology Optimization

In the case of conventional mechanism design, the objective of the topology optimization problem is to find the structure that maximizes the output work at specified locations for a given actuation energy. The location and direction of the actuator action are typically given. Without further augmentation of the problem, mechanisms with elastic hinges are formed. This is illustrated by the basic example in Fig. 3. For a given forcing input F^{in} at point A, the horizontal displacement u^{out} at point B is maximized.

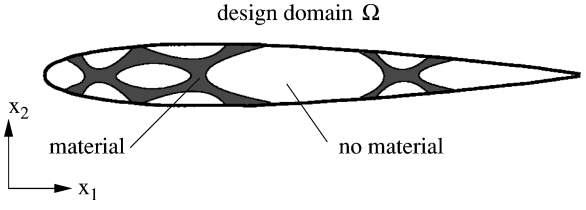

Fig. 2 Topology optimization.

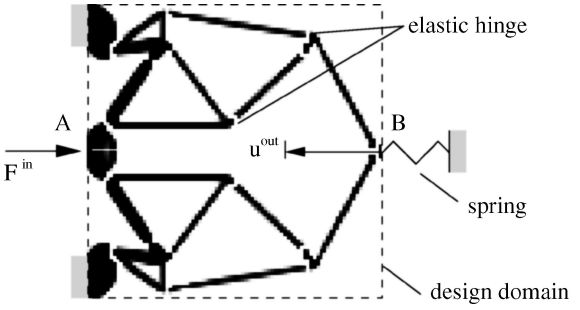

Fig. 3 Design of a mechanism by material-based topology optimization.

Topology optimization methods for mechanisms generally assume that all external loads are known *a priori* and are independent of the displacements caused by the actuators. However, a design method for mechanism systems subject to aerodynamic loading must account for the dependency of the flow on the structural deformation. This is achieved by integrating the mechanism design topology optimization into a fluid–structure analysis framework.

The design approach presented in this paper extends the recent work on topology optimization for the design of aeroelastic wing structures.[21] Therein, the layout of internal stiffeners in two- and three-dimensional wing models is optimized for minimum mass while the lift-to-weight ratio, the lift-to-drag ratio, and the maximum stress in the skin are constrained. In that work, the wing design problem essentially leads to a stiff, conventional wing design, so that the structural response can be predicted assuming small displacements. In contrast, the mechanism and airfoil skin in the present work undergo large displacements requiring a nonlinear kinematic model for predicting the structural response.

C. Design of Pivot Points and Actuation Placement

The inclusion of pivot points and actuation forces as optimization variables requires an augmentation to the mechanism design model described above. Pivot points can be modeled as hinges connecting the mechanism to the support structure. At the hinge, the translational motion of the mechanism and support structure are identical but the rotations are independent. In order to determine the location of pivots, this coupling can be treated as a design parameter. Fictitious springs are introduced that connect candidate points in the design space with points of the support structure.[40,41] The stiffness of the spring is treated as a continuous parameter that varies between two extremes: a large maximum value that essentially represents a fully coupled state and a small minimum value that allows for unconstrained motion.

In a similar fashion, the number and location of the actuators can be varied by introducing nodal forces as design parameters acting on a subset of points in the design space. Each force vector is defined by its magnitude and direction, both of which can be treated as optimization variables. In order to avoid a large number of actuators, the force magnitude $\|\boldsymbol{F}_i^{\text{act}}\|$ of the ith actuator is defined by a nonlinear function of a resource parameter $r_i \in \{\Re | \, 0 \leq r_i \leq 1\}$ and the overall actuation resource $\sum_i r_i$ is constrained,

$$\left\|\boldsymbol{F}_i^{\text{act}}\right\| = F_i^{\max} r_i^{\beta}, \qquad \sum_i r_i \leq N^{\text{act}} \tag{3}$$

where $F_i^{\max}$ is the maximum force generated by the actuator and N^{act} is the maximum number of actuator. Similarly to the SIMP approach (2), the nonlinearity in (3) discourages intermediate force magnitudes. In addition, in order to account for the characteristics of a specific actuator type, the output energy of an actuator can be constrained, along with the maximum force output and stroke.

D. Design Model

The proposed topology optimization process introduces three variable types: density variables describing the material distribution of the mechanism, stiffness variables representing the variable coupling between mechanism and support structure, and force variables defining the magnitude and direction of the actuator forces. A design domain can be defined for each variable type as depicted in Fig. 4 where the design domains partially overlap.

The material distribution in the mechanism design domain is discretized by a finite element mesh. The material state of each element

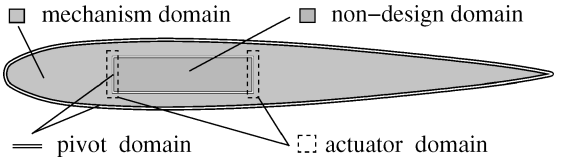

Fig. 4 Design domains for airfoil mechanism designs.

is defined by one optimization variable, using the SIMP interpolation scheme. The stiffness of each spring attached to every node in the pivot design domain is described by one optimization variable. To obtain a smooth, nonjagged material boundary and to capture geometric details of the mechanism structure, a high-resolution discretization of the density distribution is needed. This leads to a dense mesh with a large number of optimization variables and an even larger number of finite element degrees of freedom. The number of optimization variables is further increased by the number of force variables.

E. Solution Method

As stated above, the design model leads to a large number of optimization and state variables.The coupled fluid–structure response is governed by a system of coupled nonlinear equations that form a large set of equilibrium constraints. These constraints, along with the coupled fluid–structure state variables, can be eliminated by satisfying the coupled state equation for each set of design optimization variables. This approach, called nested analysis and design, is adopted in this study as it allows the designer to reuse existing analysis tools and limits the size of the optimization problem.

Assuming that the optimization criteria are smooth functions of the design variables, the resulting optimization problem can be solved by gradient-based methods. Sequential convex programming (SCP) methods, in particular the method of moving asymptotes (MMA), are frequently applied to complex structural and coupled electro-thermal-mechanical topology optimization problems.[42–45] For aeroelastic topology problems a sequential augmented Lagrange (SAL) procedure in combination with a limited-memory quasi-Newton algorithm presents an interesting alternative.[20,21] Both SCP and SAL methods have strengths and weaknesses and either may be more efficient depending on the particular problem. In the current study, an MMA algorithm with a conservative strategy for adapting the asymptotes and a step size control is applied.

III. Coupled Fluid–Structure Analysis and Sensitivity Analysis

In each step of the optimization procedure, the optimization algorithm calls for the evaluation of the optimization criteria, c_j, and their gradients with respect to the optimization variables, $\mathrm{d}c_j/\mathrm{d}s_i$. As the optimization criteria in general depend on the fluid–structure response, the coupled fluid–structure equilibrium needs to be computed for each design.

A. Coupled Fluid–Structure Analysis

In this work, the fluid–structure response of the adaptive system is predicted by coupling a three-dimensional finite volume method approximating an Euler flow and a nonlinear elastic finite element method for structural components. More specifically, a three-field formulation of the coupled response is employed as it allows for large motion of the fluid mesh.[46] The deformations imposed on the fluid–structure interface by the structure need to be propagated into the computational fluid domain in order to maintain a valid fluid mesh. For this purpose, the motion of the fluid mesh is described by the deformation of a fictitious structure due to prescribed displacements on the fluid–structure interface, leading to a third set of equations. The discrete form of the coupled fluid/structure/moving-mesh system for steady-state conditions can be written as follows:

$$\mathcal{S}(\boldsymbol{s},\boldsymbol{u},\boldsymbol{v},\boldsymbol{w})=\boldsymbol{0} \tag{4}$$

$$\mathcal{D}(\boldsymbol{s},\boldsymbol{u},\boldsymbol{v})=\boldsymbol{0} \tag{5}$$

$$\mathcal{F}(\boldsymbol{s},\boldsymbol{v},\boldsymbol{w})=\boldsymbol{0} \tag{6}$$

where $\boldsymbol{s}$ is the vector of design variables and $\boldsymbol{u}$, $\boldsymbol{v}$, and $\boldsymbol{w}$ are the structural displacements, motion of the fluid grid points, and fluid state variables, respectively.

In this work, the structural equilibrium (4) is described by a corotational finite element formulation[47] that accounts for large displacements and rotations of the mechanism. The motion of the fluid mesh (5) is modeled by a robust nonlinear spring-analogy model.[48] The fluid residual $\mathcal{F}$ is the vector of arbitrary Lagrangian–Eulerian Roe fluxes resulting from a volume discretization of the Euler flow equations.

The coupled system of Eqs. (4–6) is solved by a staggered procedure that decomposes the coupled system into fluid and structural subdomains and allows the application of different solution methods to the individual subproblems. The reader is referred to Maute et al.[14] for a detailed discussion of the coupled system and the specific staggered algorithm employed in this study.

B. Adjoint Sensitivity Analysis

Because the number of optimization variables is large ($>10^3$) and the evaluation of the coupled fluid–structure response costly, an efficient and accurate sensitivity analysis is of great importance. In this study, an adjoint approach is applied to the evaluation of the gradients of the optimization criteria with respect to the optimization variables.

The gradients of the optimization criterion c_j with respect to the optimization variable s_i can be computed as follows:

$$\frac{\mathrm{d}c_j}{\mathrm{d}s_i}=\frac{\partial c_j}{\partial s_i}+\frac{\partial c_j^T}{\partial \boldsymbol{u}}\frac{\mathrm{d}\boldsymbol{u}}{\mathrm{d}s_i}+\frac{\partial c_j^T}{\partial \boldsymbol{v}}\frac{\mathrm{d}\boldsymbol{v}}{\mathrm{d}s_i}+\frac{\partial c_j^T}{\partial \boldsymbol{w}}\frac{\mathrm{d}\boldsymbol{w}}{\mathrm{d}s_i} \tag{7}$$

where the derivatives $\mathrm{d}\boldsymbol{u}/\mathrm{d}s_i$, $\mathrm{d}\boldsymbol{v}/\mathrm{d}s_i$, and $\mathrm{d}\boldsymbol{w}/\mathrm{d}s_i$ are given by differentiating the governing coupled equations (4–6), which yields

$$\begin{bmatrix}\frac{\partial\mathcal{S}}{\partial s_i}\\ \frac{\partial\mathcal{D}}{\partial s_i}\\ \frac{\partial\mathcal{F}}{\partial s_i}\end{bmatrix}+\underbrace{\begin{bmatrix}\frac{\partial\mathcal{S}}{\partial\boldsymbol{u}} & \frac{\partial\mathcal{S}}{\partial\boldsymbol{v}} & \frac{\partial\mathcal{S}}{\partial\boldsymbol{w}}\\ \frac{\partial\mathcal{D}}{\partial\boldsymbol{u}} & \frac{\partial\mathcal{D}}{\partial\boldsymbol{v}} & \boldsymbol{0}\\ \boldsymbol{0} & \frac{\partial\mathcal{F}}{\partial\boldsymbol{v}} & \frac{\partial\mathcal{F}}{\partial\boldsymbol{w}}\end{bmatrix}}_{\mathcal{A}}\begin{bmatrix}\frac{\mathrm{d}\boldsymbol{u}}{\mathrm{d}s_i}\\ \frac{\mathrm{d}\boldsymbol{v}}{\mathrm{d}s_i}\\ \frac{\mathrm{d}\boldsymbol{w}}{\mathrm{d}s_i}\end{bmatrix}=\boldsymbol{0} \tag{8}$$

where $\mathcal{A}$ denotes the Jacobian of the coupled problem.

Equations (7) and (8) are evaluated following the adjoint approach:

$$\frac{\partial c_j}{\partial s_i}=\frac{\partial c_j}{\partial s_i}-\begin{bmatrix}\boldsymbol{a}_u\\ \boldsymbol{a}_v\\ \boldsymbol{a}_w\end{bmatrix}_j^T\begin{bmatrix}\frac{\partial\mathcal{S}}{\partial s_i}\\ \frac{\partial\mathcal{D}}{\partial s_i}\\ \frac{\partial\mathcal{F}}{\partial s_i}\end{bmatrix} \tag{9}$$

The adjoint solution $\boldsymbol{a}_j=\{\boldsymbol{a}_u,\boldsymbol{a}_v,\boldsymbol{a}_w\}_j$ associated with the optimization criteria c_j is defined as follows:

$$\begin{bmatrix}\boldsymbol{a}_u\\ \boldsymbol{a}_v\\ \boldsymbol{a}_w\end{bmatrix}_j=\mathcal{A}^{-T}\begin{bmatrix}\frac{\partial c_j}{\partial\boldsymbol{u}}\\ \frac{\partial c_j}{\partial\boldsymbol{x}}\\ \frac{\partial c_j}{\partial\boldsymbol{w}}\end{bmatrix} \tag{10}$$

The coupled linear problem (10) for computing the adjoint response $\boldsymbol{a}_j$ is solved by a Gauss–Seidel type of staggered procedure. The reader is referred to Maute et al.[49] for a detailed discussion of the numerical complexity of the adjoint approach and computational performance of the staggered algorithm.

IV. Numerical Experiments

The proposed design methodology for shape-adaptive wings is illustrated by numerical experiments conducted on a fictional design problem shown in Fig. 5. The design problem is to find the mechanism layout and actuation system that deform a quasi three-dimensional wing section from a default NACA 0012 airfoil into a shape that produces an optimal lift-to-drag (L/D) ratio.

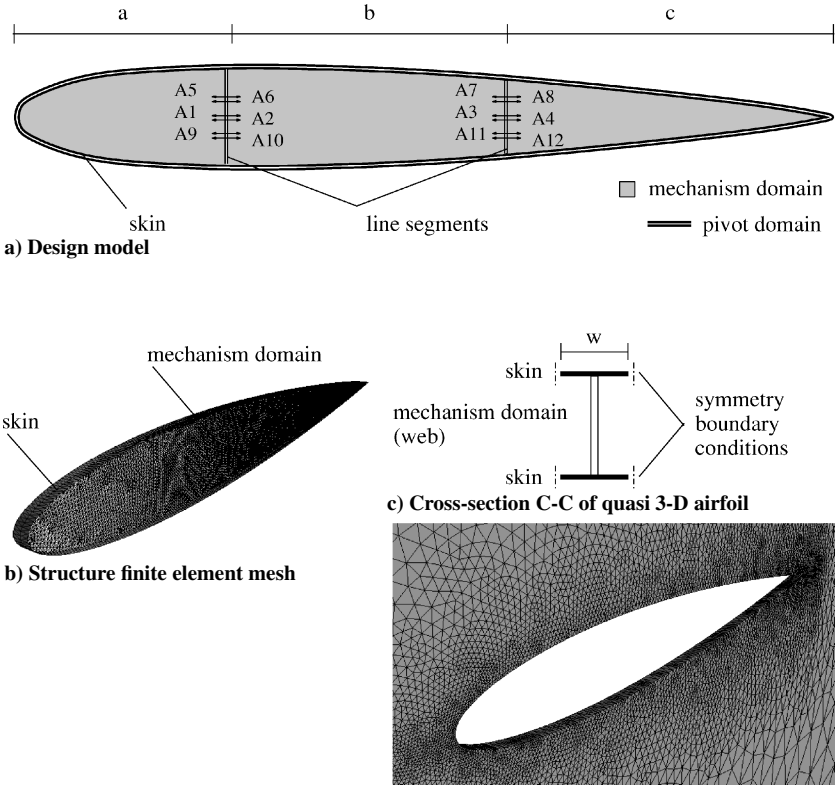

Fig. 5 Model problem for numerical experiments.

The quasi three-dimensional airfoil section is modeled by a thin-walled web which is enclosed by a strip of constant thickness representing the skin. The web constitutes the two-dimensional design domain for the mechanism. The skin serves mainly the purpose of transferring the aerodynamic pressure onto the web. Symmetry boundary conditions are applied along the edges of the shell strip and to the computational fluid domain enclosing the airfoil. The authors note that this problem could be modeled more efficiently by a two-dimensional model. However, for the present study the adjoint aeroelastic sensitivity analysis outlined above was available only within a three-dimensional fluid code[49] and therefore the above quasi three-dimensional model was developed for illustrating the proposed design methodology.

The design domain for the mechanism is discretized by 4314 quadrilateral design patches.The mechanism can be attached at 50 potential pivot points to two vertical line segments representing the intersection of front and rear spars with the airfoil section. A maximum number of 12 locations for potential actuators are available. These locations are labeled A1–A12 in Fig. 5a. For the sake of simplicity, it is assumed that each actuator can only generate a force in the horizontal direction.

The geometric and material properties defining the problem are summarized in Tables 1a and 1b. The airfoil has an overall length of 2.3 m. The thickness of the web is 0.005 m, that of the skin is 0.002 m, and the effective width of the airfoil section is 0.05 m. Aluminum has been selected as the material for the mechanism and the skin. The freestream conditions correspond to a flight at 10-deg angle of attack at sea level. Three flight speeds labeled by subscripts I, II, and III are studied. The associated Mach numbers and the aerodynamic pressure values are given in Table 1c. Except in Sec. IV.B, the flight speed corresponds to $Ma_{\mathrm{I}} = 0.3$.

Three variations of this problem are studied: in case **MLO** the layout of the mechanism is determined for given sets of pivot points and actuators, in case **MPV** the location and number of pivot points are also variable, and in case **MPF** the pivot points and the location of a limited number of actuators are optimized.

For all three cases, the design constraints include the maximum mass of the mechanism, the maximum pitching moment,

Table 1 Model problem: geometry, fluid and structural parameters, and constraint values

a. Geometry		
Front segment	a	0.58 m
Mid segment	b	0.78 m
Rear segment	c	0.94 m
Width	w	0.94 m
b. Structural parameters		
Skin thickness	t_{skin}	0.002 m
Skin width	w_{skin}	0.180 m
Web thickness	t_{web}	0.005 m
Elastic modulus (bulk)	E	71.0 GPa
Poisson ratio	ν	0.25
Spring stiffness (bulk)	k	71.0 GN/m
Actuator force	F^{act}	10.0 N
c. Fluid parameters		
Angle of attack (pitch)	α	10 deg
Free-stream pressure	p_∞	101.3 kPa
Free-stream density	ρ_∞	1.225 kg/m^3
Free-stream Mach number	Ma_{I}	0.3
	Ma_{II}	0.212
	Ma_{III}	0.424
Aerodynamic pressure	q_{I}	6.384 kPa
	q_{II}	12.768 kPa
	q_{III}	3.192 kPa
d. Optimization parameters		
Maximum stroke	$u_{\max}$	0.02 m
Maximum pitch moment	$M_{\max}$	150.0 Nm
Maximum mass	$m_{\max}$	20%

and the maximum actuation stroke. The optimization problem reads:

$$\begin{aligned} \max \quad & L/D \\ \text{s.t.} \quad & M_{\mathrm{pitch}} - M_{\max} \le 0 \\ & |u_{\mathrm{stroke}}| - u_{\max} \le 0 \\ & m - m_{\max} \le 0 \end{aligned}$$

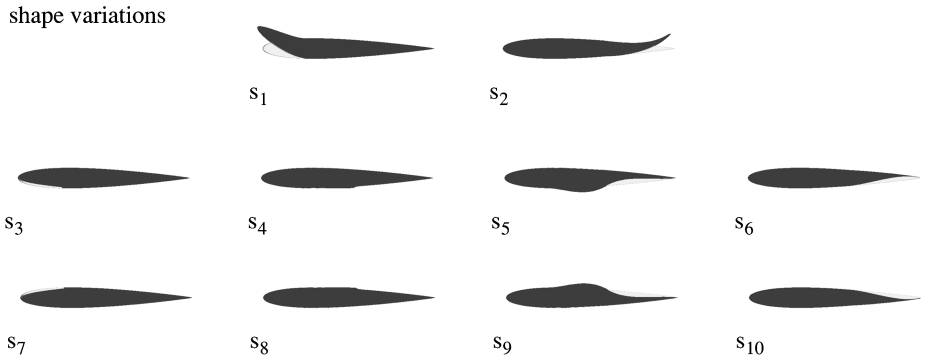

a) Aerodynamic shape optimization

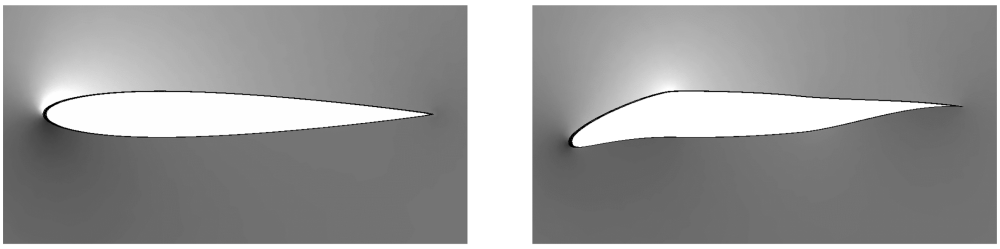

b) Initial and optimized shapes with pressure contours

Fig. 6 Two-step design procedure. Step 1: aerodynamic shape optimization.

where L and D denote the aerodynamic lift and drag, respectively; M_{pitch} is the pitching moment; u_{stroke} is the stroke of the actuators measured in the direction of the actuation forces at the actuators; and m denotes the mechanism mass. In addition, for case **MPF**, the maximum number of actuators is constrained following the SIMP-type formulation (3). The constraint limits are summarized in Table 1d. A rather small stroke limit is chosen to obtain a displacement amplifying mechanism. As the absolute value of the density is of no importance for this problem, the mass is specified relative to the mass if the entire mechanism design was filled with bulk material.

The structural mesh contains 17, 256 three-node membrane elements, where four overlapping elements with identical material properties form one design patch. The skin is generated by 1, 872 shell elements representing the wet structural surface. The aerodynamic design criteria and the aerodynamic loads are predicted by an Euler flow with added artificial viscosity. The authors note that the predicted drag is not physical but is used here for illustrative purposes. In comparison to only maximizing the lift, for example, the objective used here favors more complex aerodynamic shape changes at the nose and trailing edge. Direct inclusion of viscous effects via a Navier–Stokes flow model is needed in the future but could not be done in this study because the fluid code used has the adjoint sensitivity formulation only for an inviscid flow. The fluid computational domain is discretized by 42, 234 tetrahedron and 14, 476 grid points.

The exponent β for interpolating the material properties (2) and the actuation forces (3) is set to 3.0. The SIMP approach for finding the mechanism layout is augmented by an extended filter method to attenuate the mesh dependency of the optimization results.[20]

A. Case MLO: Mechanism Layout Optimization

To illustrate the importance of the fluid–structure interaction in the design of adaptive wings, the proposed integrated design approach of Sec. I.C is compared to the two-step procedure of Sec. I.B. In this case study, it is assumed that only the actuators at points A1–A4 are active. The actuators at points A1 and A2 generate a fixed force towards the leading edge, whereas those at points A3 and A4 actuate towards the trailing edge. The design domain for the mechanism is fixed along the vertical line segments except for points adjacent to the active actuators.

1. Application of Two-Step Procedure

Let us first consider the two-step optimization procedure described in Section I.B. The first step in the process is to solve an aerodynamic shape optimization problem, that is, to find the shape that generates maximum L/D subject to the pitching moment constraint. Structural constraints accounting for actuation limits cannot be considered in this step. The shape of the airfoil is parameterized by B-splines with 10 independent control parameters, which are the optimization variables. The basic shape variations associated with these control parameters are shown in Fig. 6a. Optimization variables s_1 and s_2 define shape variations at the leading and trailing edges, respectively. The upper airfoil shape can be changed by varying variables s_3–s_6, the lower airfoil shape through variables s_7–s_{10}.

The initial and optimal shapes resulting from the aerodynamic shape optimization are shown in Fig. 6b along with their pressure distributions. The objective is increased from 9.46 for the baseline uncambered airfoil to 13.23 for the optimal design. Note that the pitch constraint is active at the optimum, meaning that the optimizer could find a shape with better objective, but only at the expense of violating this constraint. This result is pretty much what one would expect: a cambered airfoil creates more lift, but in order not to violate the pitching moment constraint, the airfoil is in a somewhat nose-down configuration. The authors note that a finer discretization of the airfoil shape with more control parameters would most likely lead to an optimization result with a larger objective value. However, the parameterization chosen sufficiently serves the purpose of this study.

In the second step, the topology optimization problem is solved to find a mechanism that creates a deformed shape to match the aerodynamically optimal target shape. The difference between the target and the deformed shape is measured by the L_2-norm of the vector $\|\boldsymbol{x}^d_{\text{skin}} - \boldsymbol{x}^a_{\text{skin}}\|$, where $\boldsymbol{x}^d_{\text{skin}}$ denotes the position of the nodes on the skin in the deformed state and $\boldsymbol{x}^a_{\text{skin}}$ the position of the target. In this step, the constraint on the maximum stroke and the mass are included, but the aerodynamic design criteria cannot be considered. Note that the pressure load corresponding to the aerodynamic optimum shape is applied to the structure as a constant external load.

optimized density distribution
(deformed state)

a) Step 2: topology optimization

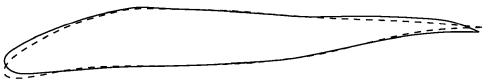

- - - - shape optimization result
—— deformed shape of actuated mechanism

b) Comparison optimization results

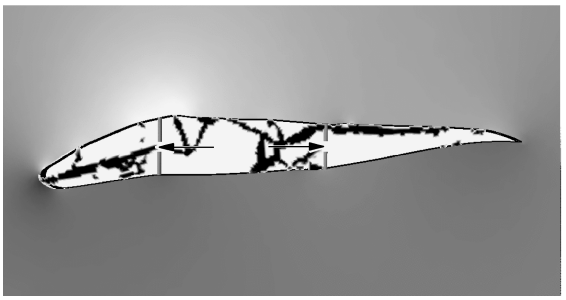

deformed configuration with
with pressure contours

c) Evaluation of aerodynamic performance

Fig. 7 Two-step design procedure. Step 2: topology optimization.

a) Density distribution—undeformed shape

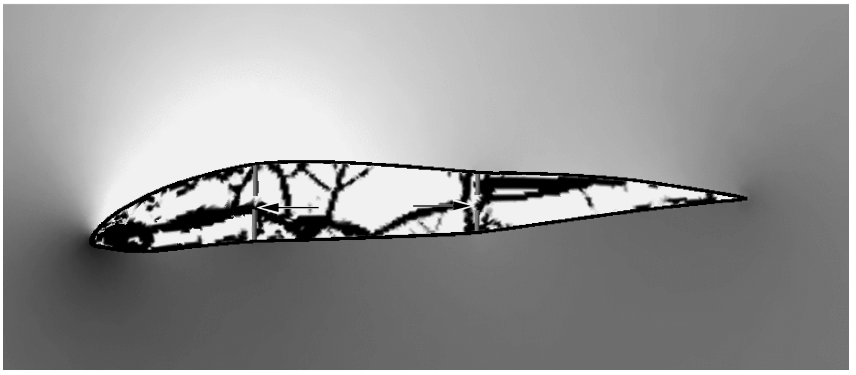

b) Deformed configuration with pressure contours

Fig. 8 Coupled fluid–structure approach.

The optimal material distribution of the topology optimization process in the deformed state is shown in Fig. 7a. The aerodynamically optimal shape and the shape obtained by the optimized mechanism are compared in Fig. 7b. The shapes match well in the middle section of the airfoil but differ noticeably in the nose and tail segments. This is clearly reflected in the aerodynamic performance of the airfoil section, which is evaluated by a coupled fluid–structure simulation (see Fig. 7c). The objective for the realized airfoil is only 11.01, a reduction of almost 17% from the result in the first step. Additionally, the pitching moment exceeds the maximum feasible moment by 55.62%.

While the decoupled procedure allows the designer to employ single-discipline design and analysis tools, these results clearly demonstrate a significant drawback of this approach. That is, the sequential approach cannot account for the dependency of the aerodynamic forces on shape variations. For traditional aeroelastic shape and thickness optimization problems, bilevel decomposition strategies exist that can attenuate difficulties due to decoupled approaches of multiphysics design problems.[50,51] Such strategies, however, are less promising for the present problem as the dependencies between structural and aerodynamic variables and design criteria are highly nonlinear and implicit.

2. *Application of Integrated Multidisciplinary Approach*

In contrast to the above result, the integrated multidisciplinary design procedure described in Sec. I.C considers aerodynamic and structural design criteria simultaneously, while the interdependency of structural variables and aerodynamics is embedded into the coupled fluid–structure formulation of the problem. The result of the optimization process produces the mechanism seen in Fig. 8a. The mechanism in the deformed state and the respective pressure distribution are shown in Fig. 8b. The objective for this design is 12.69, not quite as good as the aerodynamically optimum solution from the decoupled approach, but 15.3% better than the realized decoupled result. The constraint on the pitching moment is active at the optimum, which means that this solution is feasible.

Comparing the results obtained for the adaptive airfoil mechanism to the ones for traditional compliant mechanism design, such as shown in Fig. 3, the reader may note that the mechanism in Fig. 8

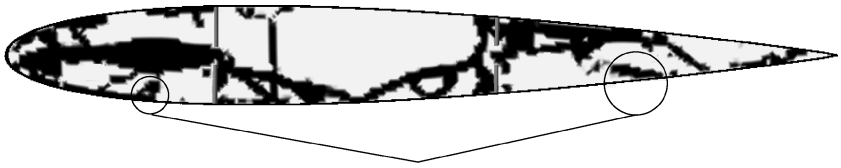

a) Case MLO/flow condition II

b) Case MLO/flow condition III

Fig. 9 Influence of aerodynamic loading on mechanism layout.

Table 2 Comparison of computational costs for two-step procedure and integrated approach

Two-step procedure		
Aerodynamic shape optimization:	Iterations	14
	CPU	3880 s
Topology optimization:	Iterations	205
	CPU	6293 s
Integrated approach	Iterations	221
	CPU	132842 s

is more bulky and that the deformation modes of are less obvious. This conceptual difference is due to the restricted design domain for the adaptive airfoil mechanism, a much smaller output displacement to input force ratio, and the distributed loading due to aerodynamic pressure.

While the integrated multi-disciplinary approach leads to an improved design over the two-step approach, it comes at the expense of larger computational costs. The number of iterations in the optimization processes and the associated CPU time required are summarized in Table 2. All computations are performed on an eight-processor personal computer cluster with double arithmetic precision. The total CPU time for the two-step approach is about 2.8 h, versus 36.9 h for the integrated approach.

B. Influence of Aerodynamic Loading on Mechanism Layout

An important design parameter for airfoil design is the aerodynamic pressure. For large aerodynamic loads the mechanism is designed to achieve the advantageous global deformations and to stiffen segments of the skin subject to large pressure loads. This leads to a rather bulky design with stiff components. As the aerodynamic pressure decreases, the mechanism design aims at fine-tuning the local deformations, leading to a layout with slender, delicate components.

The influence of the aerodynamic loading is illustrated by applying the integrated approach to the **MLO** design problem, but for the flow conditions II and III. For condition II the aerodynamic pressure is doubled and for condition III cut in half, by increasing and decreasing the Mach number, respectively. The optimized layouts are shown in Fig. 9a and b. The layout for flow condition II is quite similar to the one for the nominal case I. The mechanism for a lower dynamic pressure resembles a fishbone type of design, allowing for a local shape control. This type of design has also been proposed by Kota et al.[9]

C. Case MPV: Simultaneous Optimization of Mechanism Layout and Location of Pivots

In the above case study the boundary conditions for the mechanism are known a priori. Modeling the support structure as constraints on the displacements along the line segments significantly restricts the deformation of the airfoil. Here, the support conditions along the vertical line segments are treated as additional optimization variables, as described in Sec. II.C. As in case **MLO** the configuration of the actuators is assumed to be known.

The optimized material distribution representing the mechanism layout for this case is shown in Fig. 10. Pivot points are marked by dots. In comparison with the results shown in Fig. 8. adding the locations of pivots as optimization variables allows for significantly larger deformation, resulting in a maximum objective value of 14.30, an additional 12.69% improvement over the integrated method with fixed boundary conditions and 8.09% larger than the result obtained by aerodynamic shape optimization. As noted before, the performance of the purely aerodynamic shape optimization could be improved by refining the parameterization of the airfoil shape. This, however, does not necessarily lead to a better mechanism using the two-step procedure. The maximum pitching moment is 18.04% below the feasible limit. The authors note that this impressive performance might be misleading as deformations of the skin are extreme and most likely impractical. However, this result highlights the potential of the proposed integrated multidisciplinary design approach.

D. Case MPF: Placement of Actuators

To further improve the design, the configuration of the actuation system is included in the design process. Here, the actuator locations are also treated as optimization variables, but not their direction of action. The maximum number of actuators is set to $N^{\text{act}} = 4$ as described in Sec. II.C. The actuation forces are again acting in a horizontal direction only. In addition, the layout of the mechanism and the location of pivots are optimized simultaneously.

As the influence of the force parameters on the fluid–structure response is orders of magnitudes larger than that of the density and spring stiffness variables, the force variables converge quickly to their optimal values. However, this mismatch leads to a distorted solution space affecting the convergence of the overall optimization process. Therefore, once the optimal location of the forces has been found, the topology optimization is restarted with fixed force parameters and continued until the optimal density distribution and pivot locations are converged.

The optimized adaptive wing design for this case is depicted in Fig. 11. The locations of the pivot points are marked by dots, and the locations of active actuators are marked by arrows indicating the direction of the actuation force. Note that the actuation forces are concentrated at the middle front support, that is, points A1, A2, and A6. Only one actuator is placed at the rear support at point A11. In comparison to case **MPV**, the simultaneous optimization of the mechanism layout, the location of pivot points, and the actuation system leads to a different design. Due to the concentration of actuation forces a stiffer mechanism layout is needed in order to satisfy the stroke constraints. Here, the airfoil undergoes more of a rigid rotation than a quasi-elastic deformation. This solution might be more practical than the one found in case **MPV**. The objective

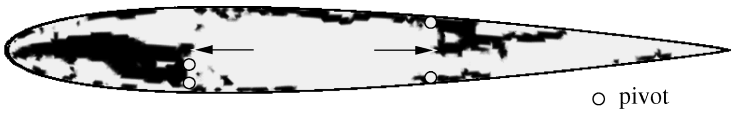

a) Density distribution—undeformed configuration

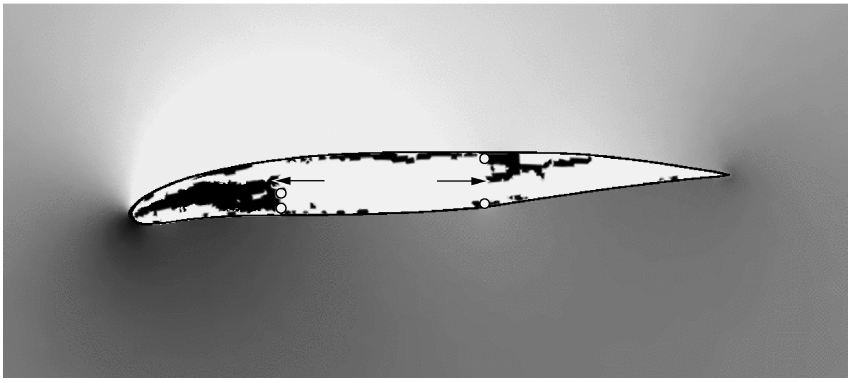

b) Deformed shape of actuated mechanism with pressure contours

Fig. 10 Coupled fluid–structure approach with pivot point optimization.

a) Density distribution—undeformed configuration

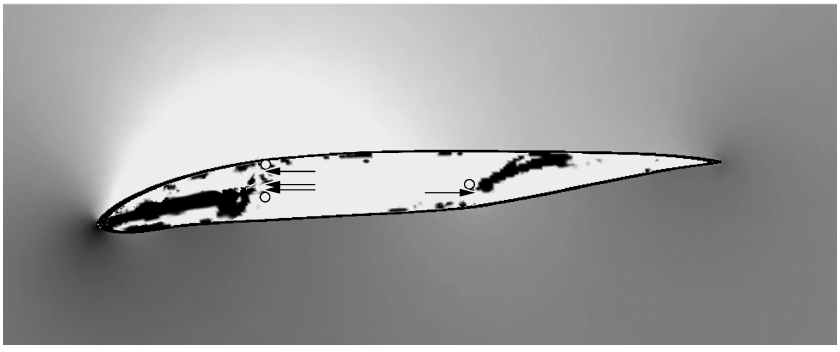

b) Deformed shape of actuated mechanism with pressure contours

Fig. 11 Coupled fluid–structure approach with pivot points and variable actuation.

for this case is 15.20 and the constraint on the pitching moment is satisfied. This objective value is larger than the one reached in case **MPV** and also significantly exceeds the performance of the two-step design.

V. Conclusions

An optimization approach for the design of adaptive wings was presented that merges topology optimization for mechanism layouts with design optimization of coupled fluid–structure problems. Finding the optimal layout of the mechanism structure was formulated as a continuous material distribution problem following the SIMP approach. The location of the pivots was varied through springs with variable stiffnesses, connecting the mechanism with the support structure. The location and direction of the actuation forces were optimized by varying the magnitude and direction of forces at potential actuator locations and introducing resource parameters that restricts the number of actuators.

The fluid–structure response was modeled by a three-field formulation. The structural response due to actuator forces and aerodynamic pressure was computed by a co-rotational finite element formulation that accounts for large displacements and rotations. For illustration purposes, the aerodynamic loads were predicted by an Euler flow with added artificial viscosity. The design sensitivities were computed by the adjoint method.

This approach was applied to the design of an adaptive airfoil section, maximizing the lift-to-drag ratio while constraining aerodynamic and structural design criteria. The optimization results showed that the proposed approach overcomes the problems of a two-step procedure decomposing the design problem into decoupled aerodynamic and structure subtasks. The dependence of the mechanism layout on the level of aerodynamic loading was illustrated. The advantages of simultaneously optimizing the mechanism layout, the location of pivot points, and the configuration of actuators were highlighted. The proposed method also allows directly imposing limits on the maximum allowable stresses, in particular for the flexible skin. The influence of this important constraint on the mechanism layout remains to be studied.

While is was shown that the proposed approach leads to an improved design over the one obtained by the two-step approach, the computational costs were more than 10 times larger. The

computational burden will further increase if the aerodynamic performance and loads are predicted by a Navier–Stokes flow model. Depending on the computational resources available, this may limit the applicability of the proposed method, in particular for the design of mechanisms for three-dimensional wing structures.

Acknowledgments

The first author acknowledges support from the National Science Foundation under Grant DMI-0348759 and the Air Force Office of Scientific Research under Grant F49620-02-1-0037. The opinions and conclusions presented are those of the authors and do not necessarily reflect the views of the sponsoring organizations. Both authors would like to thank Dr. Teri Piatt for her help in organizing and editing the paper.

References

[1]Hall, J., "Executive Summary AFTI/F-111 Mission Adaptive Wing," Tech. Rep. WRDC-TR-89-2083, Wright Research Development Center, Wright–Patterson Air Force Base, 1998.

[2]Chopra, I., "Review of State of Art of Smart Structures and Integrated Systems," *AIAA Journal*, Vol. 40, No. 11, 2002, pp. 2145–2187.

[3]Anderson, E. H., Fahey, S., and Regelbrugge, M., "High-Power Smart Material-Hydraulic Actuation," *SPIE Smart Structures and Materials Conference: Industrial and Commercial Applications of Smart Structures Technologies*, Vol. 5388, International Society for Optical Engineering, Bellingham, WA, 2004.

[4]Bridger, K., Lutian, J., Sewell, J., Kohlhafer, D., Cooke, A., and Small, G., "High-Pressure Magnetostrictive Pump Development: A Comparison of Prototype and Modeled Performance," *SPIE Smart Structures and Materials Conference: Industrial and Commercial Applications of Smart Structures Technologies*, Vol. 5388, International Society for Optical Engineering, Bellingham, WA, 2004, pp. 246–257.

[5]Reich, G., Bowman, J., and Sanders, B., "Large Area Aerodynamic Control for High-Altitude Long Endurance Sensor Platforms," *Journal of Aircraft*, Vol. 42, No. 1, 2005, pp. 237–244.

[6]Sanders, B., Eastep, F., and Forster, E., "Aerodynamic and Aeroelastic Characteristics of Wings with Conformal Control Surfaces for Morphing Aircraft," *Journal of Aircraft*, Vol. 40, No. 1, 2003, pp. 94–99.

[7]Monner, H., Hanselka, H., and Breitbach, E., "Development and Design of Flexible Fowler Flaps for an Adaptive Wing," *SPIE Smart Structures and Materials Conference: Industrial and Commercial Applications of Smart Structures Technologies*, Vol. 3326, International Society for Optical Engineering, Bellingham, WA, 1998, pp. 60–70.

[8]Lagoudas, D., Strelec, J., Yen, J., and Khan, M., "Intelligent Design Optimization of a Shape Memory Alloy Actuated Reconfigurable Wing," *SPIE Smart Structures and Materials Conference: Mathematics and Control in Smart Structures*, Vol. 3984, International Society for Optical Engineering, Bellingham, WA, 2000, pp. 338–348.

[9]Kota, S., Hetrick, J., Osborn, R., Paul, D., Pendleton, E., Flick, P., and Tilman, C., "Design and Application of Compliant Mechanisms for Morphing Aircraft Structures," *SPIE Smart Structures and Materials Conference: Industrial and Commercial Applications of Smart Structures Technologies*, Vol. 5054, International Society for Optical Engineering, Bellingham, WA, 2003, pp. 24–33.

[10]Kudva, J., Sanders, B., Pinkerton-Florance, J., and Garcia, E., "The DARPA/AFRL/NASA Smart Wing Program—Final Overview," *SPIE Smart Structures and Materials Conference: Industrial and Commercial Applications of Smart Structures Technologies*, Vol. 4698, International Society for Optical Engineering, Bellingham, WA, 2002, pp. 37–43.

[11]Bowman, J., Sanders, B., and Weisshaar, T., "Evaluating the Impact of Morphing Technologies on Aircraft Performance," *43rd AIAA/ASME/ASCE/AHS/ASC Structures, Structural Dynamics, and Materials Conference*, 2002; also AIAA 2002-1631.

[12]Lamar, J., "A Vortex-Lattice Method for the Mean Camber Shapes of Trimmed Noncoplanar Planforms with Minimum Induced Drag," NASA TN D-8090, 1976.

[13]Jameson, A., Martinelli, L., and Pierce, N., "Optimum Aerodynamic Design Using the Navier–Stokes Equations," *Theoretical and Computational Fluid Dynamics*, Vol. 10, Jan. 1998, pp. 213–237.

[14]Maute, K., Nikbay, M., and Farhat, C., "Coupled Analytical Sensitivity Analysis and Optimization of Three-Dimensional Nonlinear Aeroelastic Systems," *AIAA Journal*, Vol. 39, No. 11, 2001, pp. 2051–2061.

[15]Gumbert, C., Hou, G.-W., and Newman, P., "Simultaneous Aerodynamic Analysis and Design Optimization (SAADO) for a 3D Flexible Wing," *39th Aerospace Sciences Meeting & Exhibit*, 2001; also AIAA 2001-1107.

[16]Martins, J., and Alonso, J., "High-Fidelity Aero-Structural Design Optimization of a Supersonic Business Jet," *43rd AIAA/ASME/ASCE/AHS/ASC Structures, Structural Dynamics, and Materials Conference*, 2002; also AIAA 2002-1483.

[17]Rozvany, G. I. N., Bendsøe, M. P., and Kirsch, U., "Layout Optimization of Structures," *Applied Mechanics Reviews*, Vol. 48, No. 2, 1995, pp. 41–119.

[18]Bendsøe, M., *Optimization of Structural Topology, Shape, and Material*, Springer-Verlage, Berlin, 1995.

[19]Olhoff, N., and Eschenauer, H., "On Optimum Topology Design in Mechanics," *ECCM'99, European Conference on Computational Mechanics*, 1999, p. 71.

[20]Maute, K., Nikbay, M., and Farhat, C., "Conceptual Layout of Aeroelastic Wing Structures by Topology Optimization," *43rd AIAA/ASME/ASCE/AHS/ASC Structures, Structural Dynamics, and Materials Conference*, 2002; also AIAA 2002-1480.

[21]Maute, K., and Allen, M., "Conceptual Design of Aeroelastic Structures by Topology Optimization," *Structural and Multidisciplinary Optimization*, Vol. 27, Nos. 1–2, 2004, pp. 27–42.

[22]Ananthasuresh, G., Kota, S., and Kikuchi, N., "Strategies for Systematic Synthesis of Compliance MEMS," *Proceedings of the 1994 ASME Winter Annual Meeting*, American Society of Mechanical Engineers, New York, 1994, pp. 677–686.

[23]Sigmund, O., "On the Design of Compliant Mechanisms," *Mechanics of Structures and Machinces*, Vol. 25, No. 4, 1997, pp. 493–524.

[24]Nishiwaki, S., Frecker, M., Min, S., and Kikuchi, N., "Topology Optimization of Compliant Mechanisms Using Homogenization Method," *International Journal for Numerical Methods in Engineering*, Vol. 42, No. 3, 1998, pp. 535–559.

[25]Bruns, T. E., and Tortorelli, D. A., "Topology Optimization of Geometrically Nonlinear Structures and Compliant Mechanisms," *Proceedings of the 7th AIAA/USAF/NASA/ISSMO Symposium on Multidisciplinary Analysis and Optimization*, 1998, pp. 1874–1882; also AIAA Paper 1998-4950.

[26]Pedersen, C. B. W., Buhl, T., and Sigmund, O., "Topology Optimization of Large Displacement Compliant Mechanism," *International Journal for Numerical Methods in Engineering*, Vol. 50, No. 12, 2001, pp. 2683–2705.

[27]Padula, S., and Kincaid, R., "Optimization Strategies for Sensor and Actuator Placement," NASA TM 199 209126, 1999.

[28]Frecker, M., "Recent Advances in Optimization of Smart Structures and Actuators," *Journal of Intelligent Material Systems and Structures* (submitted for publication): Preprint of URL:http://edog.mne.psu.edu/faculty.html.

[29]Saggere, L., and Kota, S., "Static Shape Control of Smart Structures Using Compliant Mechanisms," *AIAA Journal*, Vol. 37, No. 5, 1999, pp. 572–578.

[30]Monner, H. P., "Realization of an Optimized Wing Camber by Using Formvariable Flap Structures," *Aerospace Science and Technology*, Vol. 5, No. 7, 2001, pp. 445–455.

[31]Lu, K.-J., and Kota, S., "Compliant Mechanism Synthesis for Shape-Change Applications: Preliminary Results," *SPIE Smart Structures and Materials Conference: Modeling, Signal Processing, and Control*, Vol. 4693, International Society for Optical Engineering, Bellingham, WA, 2002.

[32]Lu, K.-J., and Kota, S., "Design of Compliant Mechanisms for Morphing Structural Shapes," *Journal of Intelligent Material Systems and Structures*, Vol. 14, No. 6, 2003, pp. 379–391.

[33]Bharti, S., Frecker, M., Lesieutre, G., and Ramrakhyani, D., "Active and Passive Material Optimization in a Tendon Actuated Morphing Wing Structure," *SPIE Smart Structures and Materials Conference: Smart Structures and Integrated Systems*, Vol. 5390, International Society for Optical Engineering, Bellingham, WA, 2004, pp. 247–257.

[34]Bendsøe, M. P., "Optimal Shape Design as a Material Distribution Problem," *Structural Optimization*, Vol. 1, 1989, pp. 193–202.

[35]Rozvany, G. I. N., Zhou, M., and Birker, T., "Generalized Shape Optimization with Homogenization," *Structural Optimization*, Vol. 4, 1992, pp. 250–252.

[36]Papalambros, P., and Chirehdast, M., "Topology Design of Structures," *Integrated Structural Optimization Systems*, Kluwer Academic, Dordrecht, 1993, pp. 501–514.

[37]Maute, K., and Ramm, E., "Adaptive Topology Optimization," *Structural Optimization*, Vol. 10, 1995, pp. 100–112.

[38]Haber, R. B., Jog, C. S., and Bendsøe, M. P., "A New Approach to Variable—Topology Shape Design Using a Constraint on Perimeter," *Structural Optimization*, Vol. 11, 1996, pp. 1–12.

[39]Sigmund, O., and Petersson, J., "Numerical Instabilities in Topology Optimization: A Survey on Procedures Dealing With Checkerboards, Mesh-Dependencies and Local Minima," *Structural Optimization*, Vol. 16, No. 1, 1998, pp. 68–75.

[40]Buhl, T., "Simultaneous Topology Optimization of Structure and Supports," *Structural and Multidisciplinary Optimization*, Vol. 23, No. 5, 2002, pp. 336–346.

[41]Maute, K., and Frangopol, D., "Reliability-Based Design of MEMS Mechanisms by Topology Optimization," *Computers and Structures*, Vol. 81, Nos. 8–11, 2003, pp. 813–824.

[42]Ma, Z.-D., Kikuchi, N., Cheng, H.-C., and Hagiwara, I., "Topological Optimization Technique for Free Vibration Problems," *ASME Journal for Applied Mechanics*, Vol. 62, 1995, pp. 200–207.

[43]Duysinx, P., and Bendsøe, M. P., "Topology Optimization of Continuum Structures with Stress Constraints," *Proceedings of the 2nd World Congress of Structural and Multidisciplinary Optimization*, edited by W. Gutkowski and Z. Mróz, Institute of Fundamental Technological Research, Warsaw, 1997, pp. 527–532.

[44]Sigmund, O., "Design of Multiphysics Actuators Using Topology Optimization—Part I: One–Material Structures," *Computer Methods in Applied Mechanics and Engineering*, Vol. 190, Nos. 49–50, 2001, pp. 6577–6604.

[45]Sigmund, O., "Design of Multiphysics Actuators Using Topology Optimization—Part II: Two–Material Structures," *Computer Methods in Applied Mechanics and Engineering*, Vol. 190, Nos. 49–50, 2001, pp. 6605–6627.

[46]Farhat, C., Lesoinne, M., and Maman, N., "Mixed Explicit/Implicit Time Integration of Coupled Aeroelastic Problems: Three–Field Formulation, Geometric Conservation and Distributed Solution," *International Journal of Numerical Methods in Fluids*, Vol. 21, 1995, pp. 807–835.

[47]Nour-Omid, B., and Rankin, C. C., "Finite Rotation Analysis and Consistent Linearization Using Projectors," *Computer Methods in Applied Mechanics and Engineering*, Vol. 93, No. 3, 1991, pp. 353–384.

[48]Degand, C., and Farhat, C., "A Three-Dimensional Torsional Spring Analogy Method for Unstructured Dynamic Meshes," *Computers and Structures*, Vol. 80, Nos. 3–4, 2002, pp. 305–316.

[49]Maute, K., Nikbay, M., and Farhat, C., "Sensitivity Analysis and Design Optimization of Three-Dimensional Nonlinear Aeroelastic Systems by the Adjoint Method," *International Journal for Numerical Methods in Engineering*, Vol. 56, No. 6, 2003, pp. 911–933.

[50]Sobieszczanski-Sobieski, J., Agte, J. S., and Sandusky, R., "Bi-Level Integrated System Synthesis," AIAA 98-4916, 1998.

[51]Sobieszczanski-Sobieski, J., Mark, S., Agte, J. S., and Sandusky, R., "Advancement of Bi-Level Integrated System Synthesis (BLISS)," *38th AIAA Aerospace Sciences Meeting and Exhibit*, 2000; also AIAA 2000-0421.